ACS APPLIED MATERIALS & INTERFACES

Research Article

www.acsami.org

Solution-Processed Inorganic–Organic Hybrid Electron Injection Layer for Polymer Light-Emitting Devices

Takayuki Chiba,[‡] Yong-Jin Pu,*[,†,‡] Masakatsu Hirasawa,[‡] Akito Masuhara,[‡] Hisahiro Sasabe,[†,‡] and Junji Kido*[,†,‡]

[†]Department of Organic Device Engineering and [‡]Research Center for Organic Electronics, Yamagata University, 4-3-16 Jonan, Yonezawa, Yamagata 992-8510, Japan

Supporting Information

ABSTRACT: A lithium quinolate complex (Liq) has high solubility in polar solvents such as alcohols and can be spin-coated onto emitting polymers, resulting in a smooth surface morphology. A polymer light-emitting device fabricated with spin-coated Liq as an electron injection layer (EIL) exhibited a lower turn-on voltage and a higher efficiency than a device with spin-coated Cs_2CO_3 and a device with thermally evaporated Ca. The mixture of ZnO nanoparticles and Liq served as an efficient EIL, resulting in a lower driving voltage even in thick films (~10 nm), and it did not require a high-temperature annealing process.

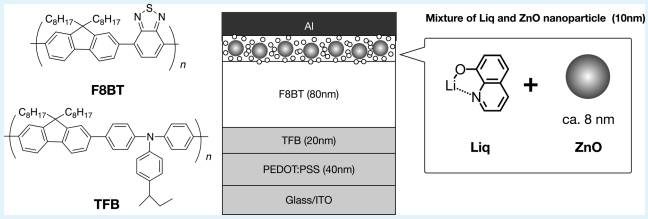

KEYWORDS: *polymer light-emitting device, solution process, electron injection, lithium quinolate, ZnO nanoparticles, inorganic–organic hybrid*

1. INTRODUCTION

Polymer light emitting devices (PLEDs) prepared using solution processes, such as slot die coating and gravure printing, are advantageous for large-scale devices because of their low fabrication cost.[1,2] Conventional PLEDs employ a highly reactive, low work function metal, such as Cs, Ba, or Ca, as an electron injection layer (EIL) and a cathode to enhance the electron injection to the emitting layer. However, the EIL and the cathode are highly reactive with atmospheric oxygen and moisture, which results in degradation of the device. The high reactivity of the EIL and the cathode makes it difficult to handle these devices in air. To avoid these problems, stable alkali metal fluorides, such as LiF or CsF, are commonly used in the EIL of dry-processed organic light emitting devices (OLEDs). Cs_2CO_3 has been reported to be an effective EIL material in solution-processed OLEDs because it is soluble in alcohol solvents and can be coated from solution. The solution-processed Cs_2CO_3 EIL exhibits a high electron injection ability that is comparable to that of alkali metals.[3,4] However, Cs_2CO_3 still has some disadvantages; it is hygroscopic and unstable in air, and it requires an ultrathin thickness because it is an insulating material. A strong chemical reduction is known to occur between Cs_2CO_3 and the thermally evaporated Al cathode. Because of this chemical reduction, the thickness of Cs_2CO_3 must be extremely thin, no thicker than 2 nm, to fully react with the evaporated Al.[4] However, the ultrathin requirement makes it difficult to obtain a uniform thickness and reproducible performance of the device. We previously reported that several lithium phenolate complexes could be used to form an excellent EIL and that the device performance was much less sensitive to the thickness of the coating of these complexes because of their electron-transporting ability.[5,6] The lithium phenolate complexes also have stability against oxidation and are less hygroscopic.

In contrast, nanocrystalline metal oxides, such as TiO_2,[7−10] ZnO,[11−21] and ZrO_2,[22] have recently been reported to be air-stable electron injection materials in PLEDs. In general, nanocrystalline metal oxide films are fabricated by spray pyrolysis deposition onto ITO substrates using metal oxide precursors. This process requires a high annealing temperature (200−450 °C)[7,9−22] to obtain highly crystalline states and high mobility in the metal oxides. Because of this requirement for high annealing temperatures, nanocrystalline metal oxides are often used in inverted PLEDs, in which they are deposited onto thermally stable ITO substrates and enhance the electron injection from the ITO into the EML. Nonhydrolytic sol–gel processing of the nanocrystalline metal oxides can avoid high annealing temperatures and deposit controlled nanosized particles onto a polymer layer at ambient temperature.[23,24] In this study, we report the efficient solution processing of an EIL based on the lithium quinolate complex (Liq); in this EIL, a low driving voltage and improved stability of the PLEDs is achieved. Liq has high solubility in polar solvents, such as alcohols, and it has a smooth surface morphology. Therefore, Liq can be spin-coated onto the emitting polymer; the device prepared with spin-coated Liq as an EIL exhibited a lower turn-on voltage and had a higher efficiency than the devices prepared with spin-coated Cs_2CO_3 or with thermally evaporated Ca and

Received: August 21, 2012
Accepted: October 22, 2012
Published: October 22, 2012

 © 2012 American Chemical Society

Liq as an EIL. A smooth film can be formed using a mixture of ZnO nanoparticles and Liq using the solution process without a high-temperature annealing process; the resultant film exhibits better stability in air, and even the thick film (~10 nm) worked efficiently as an EIL in PLEDs (Figure 1).

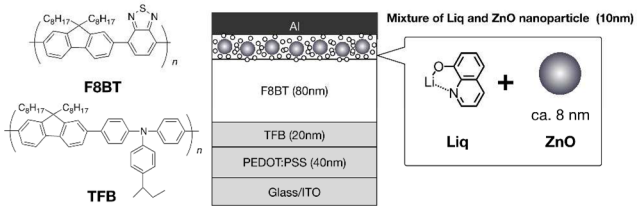

Figure 1. The chemical structure of Liq and the struture of the device.

2. RESULTS AND DISCUSSION

The multilayer PLEDs were fabricated using solution-processed Liq and Cs_2CO_3, and they were compared with PLEDs that were fabricated with thermally evaporated Ca and Liq. Poly(3,4-ethylenedioxythiophene) blended with poly(styrenesulfonate) (PEDOT:PSS) was used as an HIL, and poly(9,9-dioctyl-fluorene-*co*-*N*-(4-butylphenyl)-diphenylamine) (TFB) was used as a hole-transporting and electron-blocking layer (EBL). Poly(9,9-dioctylfluorene-*alt*-benzothiadiazole) (F8BT) was used as an EML. TFB has high hole mobility[25] and a low lowest unoccupied molecular orbital (LUMO) level (2.6 eV). The LUMO level of F8BT is 3.5 eV; thus, TFB improves electron blocking from F8BT and also acts as an exciton-blocking layer from direct quenching by PEDOT:PSS. TFB was spin-coated from a toluene solution onto the PEDOT:PSS layer and then annealed at 180 °C for 1 h in a glovebox followed by rinsing with toluene to remove the remaining soluble part of TFB, of which the thickness was ~20 nm.[26] Then, F8BT was spin-coated from *p*-xylene solution onto the TFB layer and dried successively. Afterward, Liq or Cs_2CO_3 was spin-coated from a 2-ethxyethanol solution onto the F8BT layer to serve as an EIL without redissolving F8BT. However, it is difficult to control the ~1 nm thickness that is required for the efficient EIL using solution processes such as spin coating. Therefore, the key to obtaining a thin and uniform EIL is the concentration of the solutions. We obtained a 10 nm-thick layer of Liq by spin-coating a 1% w·v^{-1} 2-ethoxyethanol solution; however, this layer was too thick to function as an EIL. Therefore, various concentrations (0.05−0.5%w·v^{-1}) of the Liq solution were tested to obtain the optimal thickness. The 0.1% solution exhibited device performance that was almost similar to that of the 0.2% solution, and the further diluted 0.05% solution decreased the device performance because there was almost no deposition onto the F8BT. The thicker 0.5% solution exhibited a much higher driving voltage. Therefore, the solution that was diluted five times (0.2% w·v^{-1}) was spin-coated to obtain a Liq layer that was thick enough to serve as an EIL.

Electroluminescence (EL) was only observed from F8BT, and no emission was observed from TFB. This result indicates that the hole and the electron are completely confined within F8BT and that the recombination of the charge carriers takes place only in the F8BT. Figure 2a presents the current density−voltage−luminance (J−V−L) characteristics of these devices. The device that was spin-coated with 1 nm Liq exhibited lower driving voltages of 2.8 V at 100 cd·m^{-2} and 3.5 V at 1000 cd·m^{-2} than those of the devices with an EIL of 5 nm Ca or 1

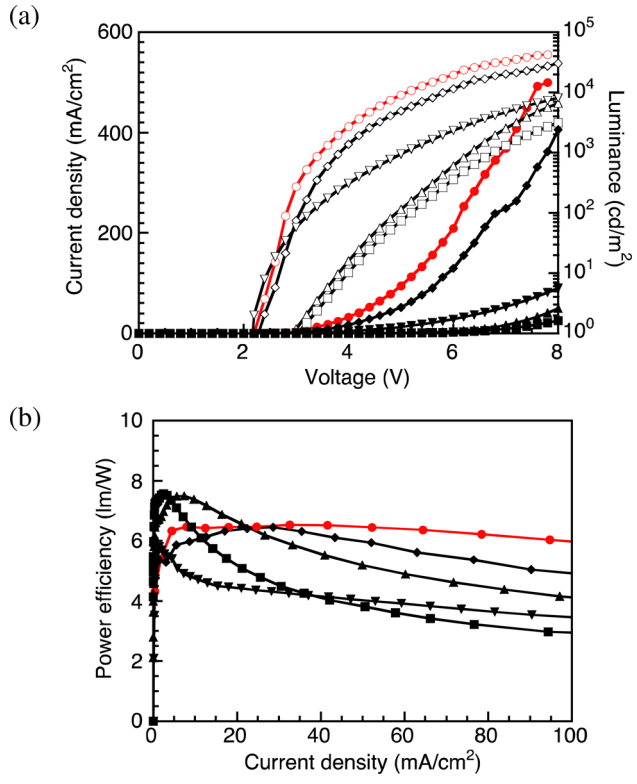

Figure 2. (a) Current density−voltage (solid symbol) and luminance−voltage (open symbol) plots. (b) Power efficiency−current density plots of the PLEDs with the following device structures: ITO/PEDOT:PSS/TFB/F8BT/spin-coated Liq (circle), evaporated Liq (upper triangle), evaporated Ca (rhombic), or spin-coated Cs_2CO_3 (lower triangle)/Al, and ITO/PEDOT:PSS/TFB/F8BT/pure 2-ethoxyethanol/evaporated Liq (square).

nm Cs_2CO_3, which demonstrates the superior electron injection property of Liq to the conjugated polymer in a solution process. In contrast, the device with thermally evaporated 1 nm Liq exhibited higher driving voltages of 5.1 V at 100 cd·m^{-2} and 6.5 V at 1000 cd·m^{-2} than those of the device with the spin-coated Liq. We investigated solvent effect[27] for the electron-injection property from the cathode to the F8BT, by spin-coating only pure 2-ethoxyethanol onto the F8BT layer before thermally evaporated Liq. The device with pure solvent treated F8BT exhibited almost the same driving voltages compared with the device without the solvent treating (Figure 2a). This result suggested that the spin-coating solvent did not affect the electron injection performance of this device. The AFM images of the thermally evaporated Liq and spin-coated Liq on the underlying F8BT film are shown in Figure S1, Supporting Information. The F8BT films exhibited a smooth surface, with an average surface roughness (Ra) of 0.26 nm. The thermally evaporated Liq showed a Ra of 1.0 nm, and the Liq spin-coated on the F8BT layer showed a smaller Ra of 0.88 nm and had a more uniform surface than the thermally evaporated Liq. The power efficiency−current density (PE-J) is shown in Figure 2b. At a luminance of 1000 cd·m^{-2}, the device with spin-coated Liq exhibited a high power efficiency of 6.6 lm W^{-1}, which is comparable to that of the device with Ca and higher than that with Cs_2CO_3; this arises because of the lower driving voltage due to the improvement of electron injection. On the other hand, the current efficiency and external quantum efficiency were not higher than those of the device with

dx.doi.org/10.1021/am301732m | ACS Appl. Mater. Interfaces 2012, 4, 6104−6108

Cs_2CO_3 because the efficient electron injection of Liq degrades the charge balance, thereby decreasing the EQE. The stability in air of the EIL is one of the important issues for the fabrication process and device stability; the conventional low-work function and alkali metals used for EILs are extremely unstable in air. We investigated the air stability of the Liq and Cs_2CO_3 EILs. These EILs were spin-coated onto F8BT in an N_2-filled glovebox, and then, the substrates were taken out and kept at a temperature of 25 °C and a humidity of 45% in air for 30 min before evaporation of the Al cathode. At a current density of 25 $mA{\cdot}cm^{-2}$, the device with the Liq EIL that was exposed to air exhibited a driving voltage shift of 2.3 V, which was much less than the 3.2 V of the device with Cs_2CO_3, compared with the devices that were not exposed to air (Figure 3a). The emission

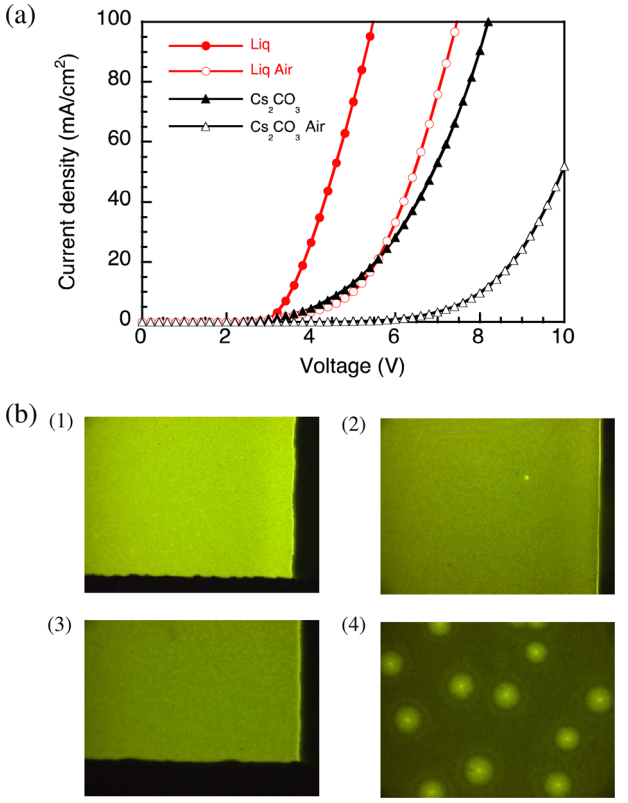

Figure 3. (a) Air stability characteristics of the device with Liq (circle) or Cs_2CO_3 (triangle). Closed symbol: without air exposure. Open symbol: with air exposure. (b) Emission images of the device with (1) Liq without air exposure, (2) Liq with air exposure, (3) Cs_2CO_3 without air exposure, and (4) Cs_2CO_3 with air exposure.

images of the device with Liq and Cs_2CO_3 are shown in Figure 3b. The device with the Liq EIL that was exposed to air exhibited unchanged emission image, compared with the devices that were not exposed to air. On the other hand, the device with Cs_2CO_3 was strongly affected by atmospheric moisture and oxygen. These results suggested that Liq is relativity stable in the presence of oxygen and moisture.

To improve the electron injection ability of the solution processed EIL that had a thickness of 10 nm, we utilized ZnO nanoparticles as a host for Liq or Cs_2CO_3. Metal oxides such as ZnO and TiO_2 can enhance the electron injection characteristics through the addition of alkali metal salts.[15,23] The ZnO nanoparticles, which were synthesized from a zinc acetate precursor,[28] were well dispersed into 2-ethoxyethanol at a concentration of 1.0% $w{\cdot}v^{-1}$. The ZnO nanoparticles were characterized using X-ray diffraction (XRD), which confirmed the formation of a wurtzite-type crystalline phase (Figure S2a, Supporting Information).[29] No absorption in the visible region was observed in the UV−vis spectra (Figure S2b, Supporting Information).[29] The average diameter of the ZnO nanoparticles was estimated using transmission electron microscopy (TEM) and dynamic light scattering (as shown in Figure S2c,d, Supporting Information) and was approximately 8 nm, with the particles being monodispersed. The ZnO particles doped with 10 mol % Liq or Cs_2CO_3 were obtained by mixing a 1% $w{\cdot}v^{-1}$ ZnO solution with a 0.2% $w{\cdot}v^{-1}$ Liq or Cs_2CO_3 solution with the same volume ratio. These dispersions of ZnO and ZnO with Liq or Cs_2CO_3 were stable for more than 6 months, and they did not precipitate ZnO. The roughness of the ZnO and the ZnO:Liq on the underlying F8BT film was measured using AFM, as shown in Figure 4a,b. The ZnO nanoparticles were

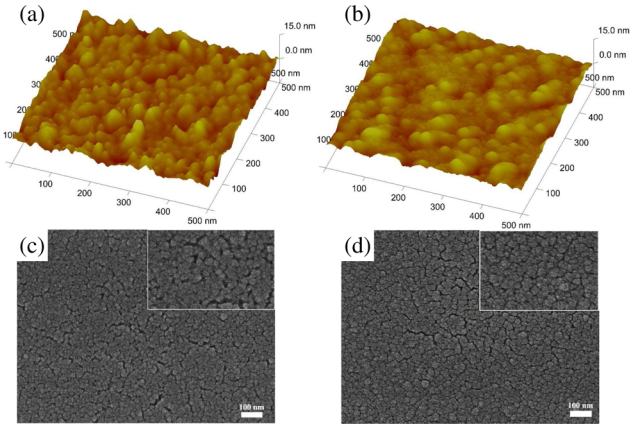

Figure 4. (a) AFM images of spin-coated ZnO and (b) spin-coated ZnO:Liq. (c) SEM images of spin-coated ZnO and (d) spin-coated ZnO:Liq.

deposited homogenously onto a F8BT layer with a Ra of 1.5 nm and the domain size was approximately 30−40 nm. The surface of the ZnO:Liq films became smooth (Ra of 0.9 nm) compared to that of the surface of ZnO, and it showed an increased domain size (approximately 50 nm). In addition, the scanning electron microscopy (SEM) images of the ZnO and ZnO:Liq exhibited the same features as the AFM images, as shown in Figure 4c,d. The aggregate size of ZnO was slightly increased by doping with Liq. These results suggest that the Liq uniformly surrounds the ZnO particle through electrostatic interactions. The photoluminescence quantum efficiency (PLQE) of the F8BT films that were coated with Liq, ZnO, or ZnO:Liq were measured using an integrating sphere system at an exctation wavelength of 480 nm to investigate the exciton quenching effect of the EILs. All of the films exhibited the same PLQEs, which were 65% of the PLQE of F8BT, indicating that these EILs do not cause exciton quenching at the interface with the emitting polymer. The devices were fabricated as follows: ITO/PEDOT:PSS (40 nm)/TFB (20 nm)/F8BT (80 nm)/ZnO, ZnO:10 mol % Liq, or ZnO:10 mol % Cs_2CO_3/Al. These ZnO-based EILs were spin-coated onto the F8BT and were not annealed. The thickness of each of the EILs was approximately 10 nm. The EL spectrum was observed only from F8BT, and no other emission from other materials was observed. The devices with ZnO:Liq and ZnO:Cs_2CO_3 EILs exhibited lower driving voltages compared to the device with the ZnO EIL

dx.doi.org/10.1021/am301732m | ACS Appl. Mater. Interfaces 2012, 4, 6104−6108

because of the improved electron injection, as shown in Figure 5. The electron injection barrier between F8BT and ZnO is large,[16] which results in less efficient electron injection. The combination of ZnO and Liq significantly reduced the driving voltage and improved the power efficiency compared to only ZnO or Liq. The angular distribution of the emission from the devices was measured. Their emission patterns deviated from Lambertian behavior, and the front luminance was suppressed. This observation explains why the EQE that was estimated from the front luminance using the Lambertian assumption was underestimated. For the device with ZnO:Liq, the EQE will be over 4.5% because of the total luminous flux. To understand the origin of the improved electron injection characteristics with Liq doping, X-ray photoemission spectroscopy (XPS) was performed on the ZnO and ZnO:Liq (Figure S3, Supporting Information). Considering the device performance, it is believed that there are some changes in the energy level of ZnO that is doped with Liq. The core-level of the XPS spectra for O 1s and Zn 2p were measured for the ZnO and ZnO:Liq films. The O 1s spectra for the ZnO:Liq shifted toward a higher binding energy by 2.3 eV in comparison to the value for only ZnO. Similarly, we also observed that the Zn 2p spectra for the ZnO:Liq shifts toward a higher binding energy by 1.9 eV in comparison to the value for only ZnO, which is consistent with the O 1s results. On the basis of the O 1s and Zn 2p XPS spectra, ZnO nanoparticles were expected to adsorb Liq.

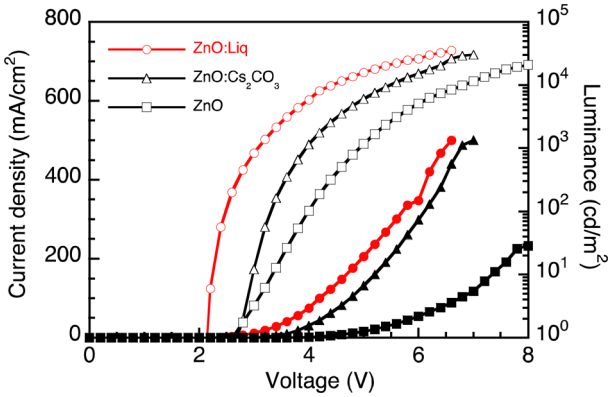

Figure 5. Current density–voltage (solid symbol) and luminance–voltage (open symbol) characteristics of ITO/PEDOT:PSS/TFB/F8BT/ZnO:Liq (circle), ZnO:Cs_2CO_3 (triangle), and ZnO (square).

We also investigated the air stability of the ZnO:Liq, and ZnO:Cs_2CO_3 EILs. At a current density of 25 mA·cm^{-2}, the device with the ZnO:Liq EIL that was exposed to air exhibited a driving voltage shift of 1.5 V, which was much less than the 3.2 V of the device with ZnO:Cs_2CO_3, compared with the devices that were not exposed to air (Figure 6). The lifetime at 50% of degradation ($T_{50\%}$) of the ZnO:Liq device was 200 h, which was longer than the 150 and 65 h lifetime of the devices with Liq and ZnO, respectively. The driving voltage of the device with Liq increased continuously, but the devices with ZnO and ZnO:Liq exhibited stable driving voltages. These results suggest that the combination of ZnO and Liq represents an effective approach for enhancing the lifetime of the device.

3. CONCLUSION

The solution-processed Liq and ZnO:Liq EILs achieved a low driving voltage and improved stability for use in PLEDs. The device with a thin spin-coated Liq as an EIL exhibited a lower driving voltage and a higher efficiency than the device with the conventional solution-processed Cs_2CO_3 because of the improved electron injection. However, the electron injection ability of Liq is still sensitive to its thickness. The mixture of ZnO nanoparticles and Liq formed a thick film with a homogeneous and smooth surface, indicating that Liq is well dispersed around the ZnO nanoparticles. This inorganic–organic hybrid EIL is an effective approach for enhancing the efficiency and stability of PLEDs, and the thickness can be sufficiently thick for reproducible large-scale devices.

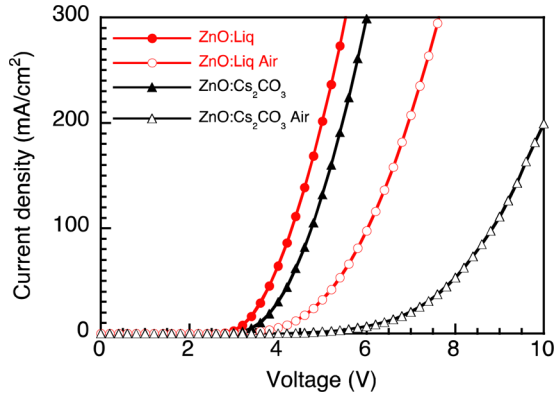

Figure 6. Air stability characteristics of the device with ZnO:Liq (circle) or ZnO:Cs_2CO_3 (triangle). Closed symbol: without air exposure. Open symbol: with air exposure.

4. EXPERIMENTAL SECTION

All devices were grown on glass substrates precoated with indium tin oxide (ITO) with a sheet resistance of 15 Ω per square. The substrates were cleaned with ultrapurified water and organic solvents and then dry-cleaned for 30 min by exposure to a UV–ozone atmosphere. PEDOT:PSS (from Starck) film (thickness ~40 nm) was spin-coated on the ITO substrates and annealed at 120 °C in air for 10 min. TFB (from American Dye Source) layers were spin-coated from a *p*-xylene solution and annealed at 180 °C for 60 min. F8BT was spin-coated using a *p*-xylene solution and annealed at 130 °C for 10 min. Liq (from eRay) and Cs_2CO_3 (from Sigma Aldrich) were spin-coated on an emissive polymer from 2-ethoxyethanol (2 mg mL^{-1}). ZnO nanoparticles were synthesized as described below. First, zinc acetate, water, and methanol were added to a flask and heated at 60 °C. Next, potassium hydroxide was dissolved into methanol and added to the flask. The mixture was stirred for 2 h and 15 min. The ZnO solution was prepared by dispersing it in 2-ethoxyethanol. The ZnO:Liq and ZnO:Cs_2CO_3 solutions were obtained by blending the ZnO solution with the Liq and Cs_2CO_3 solutions in a 1:1 volume ratio. The Al was thermally evaporated under vacuum (~10^{-4} Pa). The highest occupied molecular orbital (HOMO) energy levels were determined by atmospheric ultraviolet photoelectron spectroscopy (Rikken Keiki AC-3). The LUMO energy levels were calculated from the HOMO energy levels and the lowest energy absorption edges of the UV–vis absorption spectra. The EL spectra were taken using an optical multichannel analyzer Hamamatsu Photonics PMA-11. The current density–voltage and luminance–voltage characteristics were measured using a Keithley source measure unit 2400 and a Minolta CS200 luminance-meter, respectively. External quantum efficiencies were calculated from the front luminance, current density, and EL spectrum. The device lifetimes were measured under a constant current density of 22.5 mA/cm^2.

■ ASSOCIATED CONTENT

Supporting Information

Experimental details, XPS, and device characteristics. This information is available free of charge via the Internet at http://pubs.acs.org/.

■ AUTHOR INFORMATION

Corresponding Author

*E-mail: pu@yz.yamagata-u.ac.jp (Y.-J.P.); kid@yz.yamagata-u.ac.jp (J.K.).

Notes

The authors declare no competing financial interest.

■ ACKNOWLEDGMENTS

We would like to thank the "Strategic Promotion of Innovative R&D Program" and the "Japan Regional Innovation Strategy Program by Excellence" of Japan Science and Technology Agency (JST) for financial support.

■ REFERENCES

(1) Gong, X.; Ma, W. L.; Ostrowski, J. C.; Bazan, G. C.; Moses, D.; Heeger, A. J. *Adv. Mater.* **2004**, *16*, 615−619.
(2) Wu, H. B.; Zou, J. H.; Liu, F.; Wang, L.; Mikhailovsky, A.; Bazan, G. C.; Yang, W.; Cao, Y. *Adv. Mater.* **2008**, *20*, 696−702.
(3) Huang, J.; Li, G.; Wu, E.; Xu, Q.; Yang, Y. *Adv. Mater.* **2006**, *18*, 114−117.
(4) Huang, J.; Xu, Z.; Yang, Y. *Adv. Funct. Mater.* **2007**, *17*, 1966−1973.
(5) Endo, J.; Matsumoto, T.; Kido, J. *Jpn. J. Appl. Phys.* **2002**, *41*, L800−L803.
(6) Pu, Y.-J.; Miyamoto, M.; Nakayama, K.-i.; Oyama, T.; Masaaki, Y.; Kido, J. *Org. Electron.* **2009**, *10*, 228−232.
(7) Morii, K.; Ishida, M.; Takashima, T.; Shimoda, T.; Wang, Q.; Nazeeruddin, M. K.; Grätzel, M. *Appl. Phys. Lett.* **2006**, *89*, 183510.
(8) Lee, K.; Kim, J. Y.; Park, S. H.; Kim, S. H.; Cho, S.; Heeger, A. J. *Adv. Mater.* **2007**, *19*, 2445−2449.
(9) Bolink, H. J.; Coronado, E.; Repetto, D.; Sessolo, M.; Barea, E. M.; Bisquert, J.; Garcia-Belmonte, G.; Prochazka, J.; Kavan, L. *Adv. Funct. Mater.* **2008**, *18*, 145−150.
(10) Morii, K.; Kawase, T.; Inoue, S. *Appl. Phys. Lett.* **2008**, *92*, 213304.
(11) Bolink, H. J.; Coronado, E.; Repetto, D.; Sessolo, M. *Appl. Phys. Lett.* **2007**, *91*, 223501.
(12) Kabra, D.; Song, M. H.; Wenger, B.; Friend, R. H.; Snaith, H. J. *Adv. Mater.* **2008**, *20*, 3447−3452.
(13) Bolink, H. J.; Coronado, E.; Orozco, J.; Sessolo, M. *Adv. Mater.* **2009**, *21*, 79−82.
(14) Bolink, H. J.; Coronado, E.; Sessolo, M. *Chem. Mater.* **2009**, *21*, 439−441.
(15) Bolink, H. J.; Brine, H.; Coronado, E.; Sessolo, M. *Adv. Mater.* **2010**, *22*, 2198−2201.
(16) Kabra, D.; Lu, L. P.; Song, M. H.; Snaith, H. J.; Friend, R. H. *Adv. Mater.* **2010**, *22*, 3194−3198.
(17) Bolink, H. J.; Brine, H.; Coronado, E.; Sessolo, M. *J. Mater. Chem.* **2010**, *20*, 4047.
(18) Vaynzof, Y.; Kabra, D.; Chua, L. L.; Friend, R. H. *Appl. Phys. Lett.* **2011**, *98*, 113306.
(19) Park, J. S.; Lee, B. R.; Lee, J. M.; Kim, J.-S.; Kim, S. O.; Song, M. H. *Appl. Phys. Lett.* **2010**, *96*, 243306.
(20) Sun Park, J.; Ram Lee, B.; Jeong, E.; Lee, H.-J.; Min Lee, J.; Kim, J.-S.; Young Kim, J.; Young Woo, H.; Ouk Kim, S.; Hoon Song, M. *Appl. Phys. Lett.* **2011**, *99*, 163305.
(21) Park, J. S.; Lee, J. M.; Hwang, S. K.; Lee, S. H.; Lee, H.-J.; Lee, B. R.; Park, H. I.; Kim, J.-S.; Yoo, S.; Song, M. H.; Kim, S. O. *J. Mater. Chem.* **2012**, *22*, 12695.
(22) Tokmoldin, N.; Griffiths, N.; Bradley, D. D. C.; Haque, S. A. *Adv. Mater.* **2009**, *21*, 3475−3478.
(23) Park, M.-H.; Li, J.-H.; Kumar, A.; Li, G.; Yang, Y. *Adv. Funct. Mater.* **2009**, *19*, 1241−1246.
(24) Youn, H.; Yang, M. *Appl. Phys. Lett.* **2010**, *97*, 243302.
(25) Fong, H. H.; Papadimitratos, A.; Malliaras, G. G. *Appl. Phys. Lett.* **2006**, *89*, 172116.
(26) Kim, J.-S.; Friend, R. H.; Grizzi, I.; Burroughes, J. H. *Appl. Phys. Lett.* **2005**, *87*, 023506.
(27) Wang, Q.; Zhou, Y.; Zheng, H.; Shi, J.; Li, C.; Su, C. Q.; Wang, L.; Luo, C.; Hu, D.; Pei, J.; Wang, J.; Peng, J.; Cao, Y. *Org. Electron.* **2011**, *12*, 1858−1863.
(28) Sun, B.; Sirringhaus, H. *Nano Lett.* **2005**, *5*, 2408−2413.
(29) Beek, W. J.; Wienk, M. M.; Kemerink, M.; Yang, X.; Janssen, R. A. *J. Phys. Chem. B* **2005**, *109*, 9505−9516.